The Journal of Chemical Physics

RESEARCH ARTICLE | MARCH 09 2026

Water–ice III interfacial free energy: A mold integration study using the TIP4P/Ice model

Special Collection: Carlos Vega Festschrift

L. F. Sedano ; J. R. Espinosa ; A. R. Tejedor ; C. Vega ; E. G. Noya

J. Chem. Phys. 164, 104703 (2026)
https://doi.org/10.1063/5.0314384

The Journal of Chemical Physics ARTICLE pubs.aip.org/aip/jcp

Water–ice III interfacial free energy: A mold integration study using the TIP4P/Ice model

Cite as: J. Chem. Phys. 164, 104703 (2026); doi: 10.1063/5.0314384
Submitted: 28 November 2025 • Accepted: 11 February 2026 •
Published Online: 9 March 2026

L. F. Sedano,[1] J. R. Espinosa,[1,2] A. R. Tejedor,[1,2] C. Vega,[1] and E. G. Noya[3,a)]

AFFILIATIONS

[1] Departamento Química Física I (Unidad Asociada de I+D+i al CSIC), Fac. Ciencias Químicas, Universidad Complutense de Madrid, 28040 Madrid, Spain
[2] Yusuf Hamied Department of Chemistry, University of Cambridge, Lensfield Road, Cambridge CB2 1EW, United Kingdom
[3] Instituto de Química Física Blas Cabrera, Consejo Superior de Investigaciones Científicas (CSIC), Calle Serrano 119, 28006 Madrid, Spain

Note: This paper is part of the Special Topic, Carlos Vega Festschrift.
[a)] **Author to whom correspondence should be addressed:** eva.noya@iqf.csic.es

ABSTRACT

In this work, we evaluate the interfacial free energy, γ, between ice III and liquid water along the coexistence line for the TIP4P/Ice model using the mold integration technique. The calculated γ values exceed 40 mJ/m^2 across all the studied pressures. We observe a non-monotonic pressure dependence with a minimum appearing near 4000 bar, analogously to that observed for hexagonal ice at negative pressures. Furthermore, the interfacial free energy was determined for two different crystal planes at one pressure, revealing an anisotropy of less than 1%.

I. INTRODUCTION

The freezing of water into ice is a ubiquitous phenomenon with critical importance across disciplines.[1] Classical nucleation theory (CNT)[2,3] provides the foundational framework for understanding this phase transition, wherein the crystal nucleation barrier is critically controlled by the interfacial free energy, γ, between the forming crystal and the liquid phase.[4,5] Despite its central role, this is an elusive property whose experimental measurement is difficult, making computational methods indispensable for its determination.

Significant advances have been made in the development and application of simulation techniques to calculate γ. As recently reviewed,[6] methods such as the mold integration technique[7] have proven highly successful. This method, initially established for simple systems, has been systematically applied to quantify the ice I_h–liquid γ for various water models[8] and has been extended to other systems such as hydrates and salts.[9–12] Concurrently, estimates of γ for ice I_h have also been derived from CNT analyses of homogeneous nucleation rates,[5,13,14] showing a dependence on the thermodynamic conditions; in particular, it exhibits a non-monotonic pressure dependence, initially (at negative pressures) decreasing and then passing through a minimum,[14] a finding that is key to explaining the pressure-induced deceleration of ice nucleation. Further evidence of the existence of a minimum in γ along the I_h–water coexistence line was obtained from mold integration calculations for the planar solid–liquid interface.[15,16] In the phase diagram of water, ice III occupies the region located just above that of ice I_h in the p–T plane. The only study partially addressing the interfacial free energy of ice III is that of Espinosa *et al.*,[13] which estimated via CNT the values of γ for the ice III–fluid interface for spherical critical clusters at thermodynamic conditions out of the coexistence line. They were able to reproduce the kink observed experimentally[17,18] in the homogeneous nucleation line of water that occurs when ice III instead of ice I_h is formed in the metastable region of liquid water. However, values of γ for the ice III–water planar interface at coexistence were not reported. Notice that CNT reports values of γ for spherical critical clusters at thermodynamic conditions (p and T) away from the coexistence line, whereas the mold integration technique provides the value of γ for the planar interface at coexistence conditions.

Motivated by this gap, and building upon the extensive methodological groundwork laid by our group,[5–8,15] we present a direct computational determination of the ice III–water interfacial free energy. Using the well-established mold integration method,[7,8] we calculate γ for several thermodynamic states along the coexistence line using the 001 crystallographic plane. For one particular pressure (3000 bar), we also computed γ for the 100 plane (which is different from 001 for tetragonal symmetry). Both planes provide a similar value of γ: in fact, the difference between them (<1%) is smaller than the associated calculation uncertainty (~3%). A small value of the anisotropy (below 10%) between planes is also observed for simple systems such as hard spheres or Lennard-Jones (LJ).[19,20] Although accurately predicting interfacial free energy requires a very realistic (and likely computationally very demanding) model of water, TIP4P/Ice can provide a reasonable first estimate of the interfacial free energy for ice III. For example, for ice I_h, the interfacial free energy predicted with TIP4P/Ice is ~30 mJ/m^2, which lies well within the range of experimental values available in the literature (25–35 mJ/m^2).[8] Despite the challenges of estimating reliable nucleation rates in the absence of any prior data on the interfacial free energy of ice III, this study represents a step forward toward a more comprehensive understanding of ice nucleation kinetics.

II. METHODS

The interfacial free energy of ice III is obtained for the TIP4P/Ice potential[21] using the Mold Integration (MI) methodology,[7] succinctly explained in Sec. III B. Ice III has a tetrahedral symmetry and belongs to the $P4_12_12$ spatial group. To generate the ice configuration, we used the experimental positions of the oxygen atoms from Ref. 22 as an input for a custom program. The proton disorder is generated following the algorithm from Ref. 23 to create an initial configuration of ice III. We then run an anisotropic NpT simulation to obtain the equilibrium unit cell parameters for the model (a, b, and c). With these parameters, we created the mold configuration. It should be mentioned that the proton disorder has a small impact on the parameters of the unit cell (differences are of the order of 0.06%, i.e., of the same order as the statistical uncertainty of the simulations). Note also that the mold is generated using only the oxygen positions so that, once a water molecule falls into it, the rotation of hydrogen atoms is unconstrained. The mold is embedded into an equilibrated liquid, and simulations are run in the anisotropic Np_zT ensemble for a system of 2400 water molecules using the v-rescale thermostat[24] and the Parrinello–Raman[25] (anisotropic) barostat with relaxation times of 1 and 2 ps, respectively. Note that this ensemble (as opposed to the NpT) implies that, for each pressure, the mold must be created specifically so that we avoid any stress in the x *and* y directions of the solid. An example of the mold in the liquid is presented in Fig. 1. The number of wells and area of the mold can be found in Table II. The chosen system sizes are large enough to avoid significant system-size effects. In previous work, it has been shown that the MI method provides very similar results for the Lennard-Jones system for $N \approx 2000$ and $N \approx 6000$.[7] In addition, γ obtained for ice I_h–water (modeled with the mW potential)[8] using system sizes comparable to those employed in this work are in excellent agreement with those obtained using the capillary wave method.[26] This consistency further suggests the absence of significant finite-size effects in our current setup.

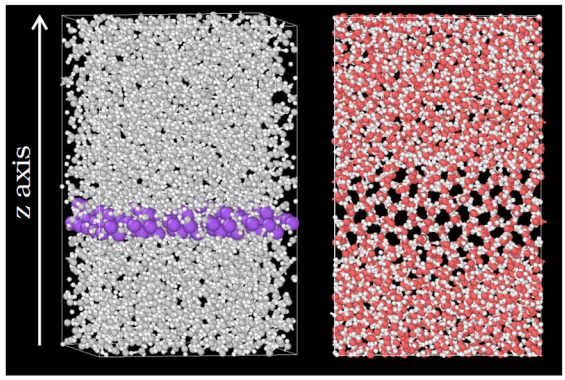

FIG. 1. Example of a liquid water configuration with the mold for a 001 plane of ice III. The mold (purple) interacts through a square well potential (only with oxygen atoms), thus trapping one water molecule in each position (well). In the right panel, the particles of the mold are not depicted in order to observe the crystalline layers formed by water molecules within and around the mold.

A time step of 1 fs was used due to the steepness of the hyperbolic tangent used to smooth the square well potential so that it can be differentiable. The parameter that controls the steepness (α) was set at 0.0017 Å (see Ref. 7 for more details). The cutoff was set at 14 Å for the electrostatic and LJ interactions, with no long-range corrections applied to the LJ potential. The particle mesh Ewald method[27,28] was employed to deal with long-range electrostatics. The LINCS[29] algorithm kept the geometry of the water molecules fixed. All the simulations were performed using the GROMACS[30] 4.6.7 package with a tabular potential in which the square potential is implemented. In addition, for the 5000 bar isobar, the interfacial free energy was also computed with the molecular dynamics open-source software LAMMPS[31] (including the mold package).[32] In these simulations, the cutoff was set at 9 Å for dispersive and electrostatic interactions, and long-range corrections (LRCs) to the energy and pressure were included. The remaining simulation parameters were unchanged, except for the use of the Nose–Hoover[33,34] thermostat and the inclusion of the SHAKE algorithm. The reason for the different cutoff is merely a technical one. The hyperbolic tangent function used to emulate a square-well potential needs a tabular form to be implemented in GROMACS (whereas it can be used analytically with the mold-integration package in LAMMPS[32]). As a technical issue, it should be pointed out that once a tabular potential is employed in GROMACS (i.e., that of the mold), all other dispersive potentials used in the simulation must also be tabular. Consequently, LRC cannot be applied to the LJ potential because, in practice, no analytical form exists for this specific case. To mitigate significant errors arising from this truncation, a larger cutoff radius must be employed. Finally, to determine the degree of crystallinity of the system, we have used the $\bar{q}_6$ order parameter[35] along with a cluster analysis program to estimate the largest cluster in the system, $n_{biggest}$ (i.e., the molecules forming the crystal layer). To minimize the mislabeling between ice III and the liquid phase, we studied different cutoff radii (r_c). Most isobars use r_c = 5 Å, which roughly corresponds to the second minimum of the radial distribution function

(see Fig. S1 and Table S1 for more details). Note that despite a consistent 2%–3% mislabeling, this is sufficient for our purposes. The MI method is independent of the order parameter, which is only used to determine if a trajectory is crystallizing during the determination of the optimal well radius.

III. RESULTS

A. Melting temperature

For the TIP4P/Ice,[21] the phase diagram has recently been reported.[36,37] The application of MI requires precise knowledge of the melting temperature (T_m) for each pressure along the coexistence line. Simulating away from the equilibrium temperature (for instance, one or two degrees above) will delay/suppress the formation of the crystal slab and, thus, hinder the proper discrimination of the critical radius. For this reason, the melting temperature for each pressure was evaluated in this work, using direct coexistence simulations for boxes containing 5600 water molecules, a system size for which the associated error is expected to lie below half a degree.[38] The semi-isotropic NpT ensemble (in which the in-plane xy and normal z directions to the interface are controlled independently, rather than the rigorously correct Np_zT) was used to avoid the risk of inducing residual stress in the solid phase. The error in the pressure associated with the surface stress[39] is of the same order as that of the stochasticity of the method, provided the longitudinal dimension (z) is large relative to the interfacial region.[40,41]

Ice III was first identified experimentally by Tammann[42] and later confirmed and refined by Bridgman.[43] Figure 2 shows that TIP4P/Ice over-stabilizes ice III when compared to the experimental results. The coexistence points for TIP4P/Ice are in good agreement with those reported by Weidmann *et al.* (in green)[36] for the same force field using the direct coexistence technique in the *NpH* ensemble. The ice III–liquid line of TIP4P/Ice runs parallel to the experimental one, with a constant offset of approximately

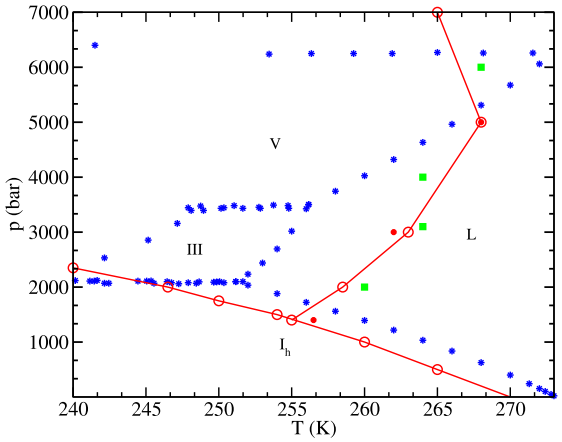

FIG. 2. Phase diagram for the TIP4P/Ice model (red circles: filled r_c = 14 Å, no LRC; open: r_c = 9 Å + standard LRC) in the relevant region of this study, compared to experimental data from Ref. 43 (blue symbols). Green symbols are *NpH* simulations for the same potential (using PME for LRC) from Ref. 36.

TABLE I. Melting points of ice III as a function of pressure for the TIP4P/Ice potential.

Pressure (bar)	T_m (K) (9 Å + LRC)	T_m (K) (14 Å)
1400	255.0	256.5
3000	263	262
5000	268	268
7000	265	265

+8 K (for the Ih–liquid, the results of TIP4P/Ice are parallel to the experimental ones with an offset of ~−3 K). A re-entrant behavior (for the ice III–fluid coexistence line) is observed close to 5000 bar and 268 K, consistent with the earlier extrapolations of Eisenberg and Kauzmann,[44] although not directly observed by them due to the metastability of ice III with respect to ice V in this region. The question of re-entrant behavior was historically proposed for I_h–liquid coexistence by Tammann,[45] a claim contested by Bridgman. Later work by other authors confirmed such re-entrant behavior in metastable regions for ices III, V, and VI,[44,46] as well as for ice I_h at negative pressures.[14,46–48]

For technical reasons, simulations involving MI require different cutoff potentials when run with GROMACS or LAMMPS (see Sec. II for discussion). This actually implies that the Hamiltonian is not identical, and therefore, the melting temperature must be calculated depending on the case. Since the majority of the results of this work have been obtained with GROMACS, the melting temperatures for a cutoff of 14 Å had to be calculated. The comparison with the standard conditions (i.e., 9 Å and long-range corrections, also from this work) is collected in Table I. The melting temperature is the roughly the same (within the error) for all cases.

B. Mold integration method

The MI method proposed by Espinosa *et al.*[7] induces the reversible creation of a crystal slab by the imposition of an attractive potential located at the equilibrium positions of the crystal plane. These empty positions are referred to as "mold," and they interact with the water molecules via a square well potential. Since we perform molecular dynamics simulations, this potential is softened using a hyperbolic tangent function in order to avoid discontinuities. The work needed to create the slab is related to the interfacial free energy, γ, such that

$$\gamma = \frac{\Delta G}{2A}, \tag{1}$$

where A is the area of the interface. The attractive potential used is simply a softened square-well potential. The interfacial free energy can be obtained by Hamiltonian integration,

$$\gamma(r_w) = \frac{1}{2A}\left(\varepsilon_{\max} N_{w,\max} - \int_0^{\varepsilon_{\max}} \langle N_{fw}(\varepsilon)\rangle_{Np_zT}\, d\varepsilon\right), \tag{2}$$

where r_w is the well's radius, A is the area of the interface, $\varepsilon_{\max}$ is the maximum interaction value of the well potential, $N_{w,\max}$ is the number of wells filled for $\varepsilon_{\max}$ (which is a number very close to the total number of wells, N_w), and N_{fw} is the number of filled wells for a certain interaction of the mold (ε). The values of N_w

TABLE II. Interfacial free energy for ice III (for the 001 plane, $L_x = L_y$, and for the 100 plane, $L_y \simeq L_z$) at different isobars using the MI technique[7] and the TIP4P/Ice[21] water model. The numbers in parentheses indicate the error (see Sec. III B for details). Notice that for a tetragonal crystal, the planes 100 and 001 are not equivalent. N_w stands for the number of wells used in the mold integration technique. The z axis is perpendicular to the plane of the interface (i.e., x, y). Values of the optimal radius of the wells r_w^o are presented.

Pressure (bar)	T_m (K)	Crystal plane	$L_x \times L_y$ (Å)	N_w	r_w^o (Å)	γ (mJ/m^2)
1400	256.5	001	1129.20	150	0.73(0.02)	45.9(1.8)
3000	262.0	001	1129.76	150	0.80(0.02)	42.7(1.8)
3000		100	1168.02	150	0.69(0.02)	42.3(1.6)
5000	268.0	001	1114.53	150	0.77(0.02)	43.7(1.6)
7000	265.0	001	1004.65	150	0.77(0.02)	45.0(1.8)

and A for each pressure are reported in Table II. Note that the free energy depends on the size of the well. We need to compute the free energy difference between the liquid with a crystal slab and the fully grown solid (or with the pure liquid, since at coexistence both phases have the same chemical potential). If the wells are too wide, the free energy of the fluid with respect to the free energy of the liquid + slab exhibits a small free energy barrier that can be overcome by thermal fluctuations. This is observed by an induction time in the growth of the slab. On the other hand, too narrow wells increase the free energy with respect to that of the ideal liquid + slab, and all the trajectories would instantly nucleate. The optimal radius for the wells (r_w^o) would correspond to the free energy of the liquid + slab. In a system with molecular (as opposed to atomistic) interactions, it is hard to discern the induction time since molecules need to reorient to form the slab. This difficulty increases with the complexity of the system[12,49] and for slow-diffusing systems.[8]

As an example, various radius sizes are presented in Fig. 3 for the 3000 bar isobar and the plane 001 exposed to the interface. For the smallest radius (r_w = 0.681 Å), the trajectories clearly form the crystal slab in the first half nanosecond. The radius r_w = 0.783 Å also shows steep increases of the biggest cluster (the slab) without any plateau. However, for 0.817 Å, one of the trajectories does not grow during the first nanosecond and is then propelled. This is the perfect example of a small barrier created by a radius $r > r_w^o$. The optimal radius corresponds to a value of r_w between regimes where all trajectories grow without induction and those where at least one trajectory stalls (i.e., around 0.8 Å in this example).

To estimate the work necessary to create the crystalline layer, we must integrate the interaction between water and the mold, avoiding the appearance of such a slab. Knowing r_w^o, the thermodynamic integration will be computed for values sufficiently larger to avoid any trajectory from escaping the minimum (ice growth) but not so big as to result in a considerable error in the extrapolation of γ at the optimal radius. The values integrated for each isobar are presented in Fig. 4 by filled symbols. The progressive increment of ε for each value of the thermodynamic integration produces a

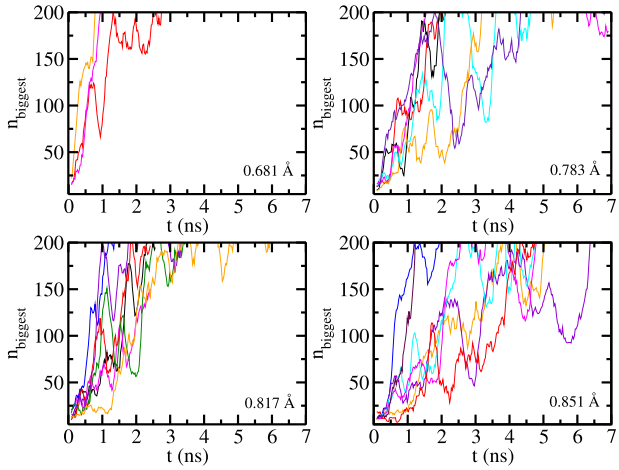

FIG. 3. Number of water molecules of the biggest cluster vs time for several trajectories and different well radii (as indicated in the legend) for the 001 plane of wells exposed at the interface at 3000 bar at the melting point (262 K).

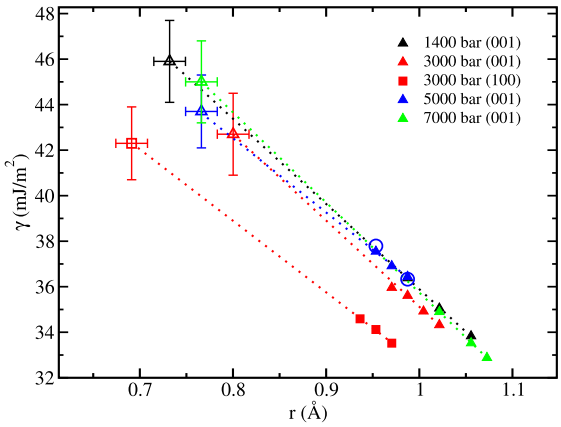

FIG. 4. Filled symbols: interfacial free energy for different values of the well radii, pressures, and crystal orientations of ice III as indicated in the legend. Dotted lines: linear fits to filled symbols. Empty symbols: extrapolation of the linear fits to the optimal well radius (r_w^o). Empty circles correspond to the results obtained using the MI with LAMMPS[32] (see Sec. III C).

sigmoidal function that can easily be integrated (see Fig. S6). The error bars for the resulting interfacial free energy were computed using the error of the slope (which takes into account the statistical error of γ at different r_w values and the sensitivity to the r_w fitting range and is shown as vertical bars) and the width of the window used to determine the optimal radii (estimated as the interval between the regime where all trajectories grow without any induction and that in which a small free energy barrier leads to some induction time for crystallization and is shown as horizontal bars).

Results for the interfacial free energy are presented in Figs. 4 and 5 and Table II. At 3000 bar, the anisotropy between the two selected crystallographic planes is very small (less than 1%). To the best of our knowledge, the anisotropy has not been studied as a function of pressure. While other, unstudied planes may exhibit larger differences, for ice I_h (at ambient pressure), the maximum anisotropic values reported lie below 10%.[50,51]

The interfacial free energy of ice III exceeds 40 mJ/m^2, a value consistent with previous observations for ices I_h and III at 2000 bar (both around 39 mJ/m^2)[13] from seeding calculations.[52,53] Note that a direct comparison must consider the methodological differences: seeding extrapolates from a spherical critical cluster to coexistence conditions, whereas MI measures γ directly for a single, specific plane. This distinction is highlighted by the 6% difference in the interfacial free energy found for the basal plane of ice I_h[15] (and the seed)[13] at 2000 bar by the same authors.

Finally, Fig. 5 shows the pressure dependence of γ at coexistence for ice I_h (from Ref. 15) and for ice III, as determined in this work. For both polymorphs, the interfacial free energy decreases with pressure, passing through a minimum value. The variation of the interfacial free energy along a coexistence line can be determined using the Gibbs–Cahn equation, which relates the change in γ to the value of the excess interfacial internal energy and to the stress.[16,54,55] Both magnitudes depend on the selected plane. However, for the particular case in which the stress and γ are similar, the excess interfacial internal energy can provide a rough idea of the magnitude of the change[16] and also a justification for the proximity of the minimum in γ to the location of the re-entrant point of the melting line.[15]

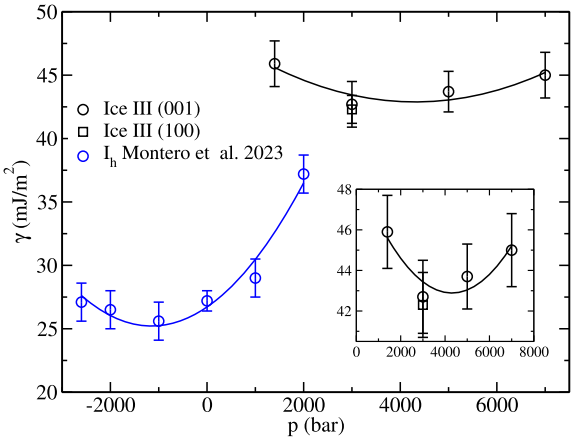

FIG. 5. Interfacial free energy vs pressure with the TIP4P/Ice water model for ice I_h (taken from Ref. 15) and for ice III, as indicated in the legend. The inset is a zoom-in of the interfacial free energy of ice III.

C. GROMACS vs LAMMPS

In this work, we compare the results for the interfacial free energy obtained with GROMACS and LAMMPS for an isobar. We deliberately choose to do it for a pressure that shows no sensitivity to the melting point with the two cutoffs used (see Table I and Sec. II for context). Figure 4 compares the thermodynamic integration for the 5000 bar isobar obtained with GROMACS 4.6.7 (filled triangles) and LAMMPS 2023 (circles), proving consistency between both software programs. The question of which software to use then relies on simplicity and computational efficiency. Admittedly, the recent implementation of the method with LAMMPS makes it user-friendly.[32] From the computational point of view, however, GROMACS outperforms LAMMPS by a factor of 1.6 when computing interfacial free energies "from scratch" (that is, without previously knowing the melting point) despite the longer cutoff; the disadvantage is that the phase diagrams are usually only known for 9 Å and long-range corrections. For the case of plain direct coexistence calculations, GROMACS outperforms (in terms of speed) LAMMPS by a factor of more than 5.5, making the former highly advisable. Simulations were performed in both cases using Intel(R) Xeon(R) Gold 6142 CPUs without GPU acceleration. However, it should be noted that the calculation of the melting points (which are often known only for the "standard" Hamiltonian) consumes almost half of the computation time of the calculation of γ using MI. Nevertheless, if the melting point for a certain potential is already known, the MI using GROMACS instead of LAMMPS is only 30% more efficient, its implementation being less straightforward.

IV. CONCLUSIONS

In this work, we investigate the interfacial free energy along the coexistence line of ice III for the 001 plane starting from the triple point (1400 bar) up to 7000 bar using the TIP4P/Ice model. We show that it is higher than that of the hexagonal ice at similar pressures[13,15] and observe a minimum of γ in its dependence on pressure, similar to what has been observed for ice I_h.[15] No anisotropy was observed between planes 001 and 100 within the error. We validate the MI implementation in LAMMPS for water and compare its performance with GROMACS, finding that the latter is 1.3 times faster for computing interfacial free energies.

SUPPLEMENTARY MATERIAL

The supplementary material encompasses Fig. S1 and Table S1, which contain the details of the $\bar{q}_6$ threshold used for each isobar. Figures S2–S5 show the evolution of the size of the largest cluster as a function of time for several trajectories that were used to determine the critical radii for all the pressures considered. Figure S6 shows the thermodynamic integration for the 001 plane. In addition, it also contains tables and a simple code to implement the mold integration using GROMACS (versions supporting tabular potentials, that is, older than 2016).

ACKNOWLEDGMENTS

We gratefully acknowledge the financial support from Grant Nos. PID2022-136919NB-C31 and PID2023-151751NB-100, funded by MICIU/AEI/10.13039/501100011033 and by FEDER, UE. L.F.S. thanks the Ministerio de Educación y Formación Profesional (MEFP) for a predoctoral Formacion Profesorado Universitario Grant No. FPU22/02900. J.R.E. acknowledges the funding from Emmanuel College, University of Cambridge, the Ramon y Cajal fellowship (Grant No. RYC2021-030937-I), the Spanish scientific plan and committee for research reference (Grant No. PID2022-136919NA-C33), and the European Research Council (ERC) under the European Union's Horizon Europe research and innovation program (Grant Agreement No. 101160499). E.G.N., J.R.E., A.T., and L.F.S. dedicate this work to Carlos Vega, who remains a constant source of inspiration.

AUTHOR DECLARATIONS

Conflict of Interest

The authors have no conflicts to disclose.

Author Contributions

L. F. Sedano: Data curation (equal); Investigation (equal); Methodology (equal); Writing – original draft (equal); Writing – review & editing (equal). **J. R. Espinosa**: Conceptualization (equal); Formal analysis (equal); Funding acquisition (equal); Methodology (equal); Supervision (equal); Validation (equal). **A. R. Tejedor**: Investigation (equal); Resources (equal). **C. Vega**: Conceptualization (equal); Funding acquisition (equal); Methodology (equal); Project administration (equal); Supervision (equal); Validation (equal). **E. G. Noya**: Conceptualization (equal); Project administration (equal); Resources (equal); Supervision (equal); Writing – original draft (equal).

DATA AVAILABILITY

The data that support the findings of this study are available within the article and its supplementary material.

REFERENCES

[1]G. C. Sosso, J. Chen, S. J. Cox, M. Fitzner, P. Pedevilla, A. Zen, and A. Michaelides, "Crystal nucleation in liquids: Open questions and future challenges in molecular dynamics simulations," Chem. Rev. **116**, 7078 (2016).

[2]J. W. Gibbs, *On The Equilibrium of Heterogeneous Substances* (Transactions of the Connecticut Academy of Arts and Sciences, 1878), Vol. 3, pp. 108–248, Continued in Vol. 16, pp. 343–524.

[3]R. Becker and W. Döring, "Kinetische behandlung der keimbildung in Übersättigten dämpfen," Ann. Phys. **416**, 719–752 (1935).

[4]S. Auer and D. Frenkel, "Prediction of absolute crystal-nucleation rate in hard-sphere colloids," Nature **409**, 1020–1023 (2001).

[5]J. R. Espinosa, A. Zaragoza, P. Rosales-Pelaez, C. Navarro, C. Valeriani, C. Vega, and E. Sanz, "Interfacial free energy as the key to the pressure-induced deceleration of ice nucleation," Phys. Rev. Lett. **117**, 135702 (2016).

[6]N. Di Pasquale, J. Algaba, P. Montero de Hijes, I. Sanchez-Burgos, A. R. Tejedor, S. R. Yeandel, F. J. Blas, R. L. Davidchack, J. R. Espinosa, C. L. Freeman, J. H. Harding, B. B. Laird, E. Sanz, C. Vega, and L. Rovigatti, "Solid-liquid interfacial free energy from computer simulations: Challenges and recent advances," Chem. Rev. **125**, 5003–5053 (2025).

[7]J. R. Espinosa, C. Vega, and E. Sanz, "The mold integration method for the calculation of the crystal-fluid interfacial free energy from simulations," J. Chem. Phys. **141**, 134709 (2014).

[8]J. R. Espinosa, C. Vega, and E. Sanz, "Ice-water interfacial free energy for the TIP4P, TIP4P/2005, TIP4P/ice and mW models as obtained from the mold integration technique," J. Phys. Chem. C **120**, 8068 (2016).

[9]J. R. Espinosa, C. Vega, C. Valeriani, and E. Sanz, "The crystal-fluid interfacial free energy and nucleation rate of NaCl from different simulation methods," J. Chem. Phys. **142**, 194709 (2015).

[10]I. Sanchez-Burgos and J. R. Espinosa, "Direct calculation of the interfacial free energy between NaCl crystal and its aqueous solution at the solubility limit," Phys. Rev. Lett. **130**, 118001 (2023).

[11]I. M. Zerón, J. M. Miguez, B. Mendiboure, J. Algaba, and F. J. Blas, "Simulation of the CO_2 hydrate-water interfacial energy: The mold integration-guest methodology," J. Chem. Phys. **157**, 134709 (2022).

[12]C. Romero-Guzmán, J. M. Zerón, J. Algaba, B. Mendiboure, J. M. Miguez, and F. J. Blas, "Effect of pressure on the carbon dioxide hydrate-water interfacial free energy along its dissociation line," J. Chem. Phys. **158**, 194704 (2023).

[13]J. R. Espinosa, A. L. Diez, C. Vega, C. Valeriani, J. Ramirez, and E. Sanz, "Ice Ih vs Ice III along the homogeneous nucleation line," Phys. Chem. Chem. Phys. **21**, 5655 (2019).

[14]V. Bianco, P. de Hijes, C. Lamas, E. Sanz, and C. Vega, "Anomalous behavior in the nucleation of ice at negative pressures," Phys. Rev. Lett. **126**, 015704 (2021).

[15]P. Montero de Hijes, J. R. Espinosa, C. Vega, and C. Dellago, "Minimum in the pressure dependence of the interfacial free energy between ice Ih and water," J. Chem. Phys. **158**, 124503 (2023).

[16]I. Sanchez-Burgos and J. R. Espinosa, "Predictions of the interfacial free energy along the coexistence line from single-state calculations," J. Chem. Phys. **161**, 204701 (2024).

[17]C. A. Angell and H. Kanno, "Density maxima in high-pressure supercooled water and liquid silicon dioxide," Science **193**, 1121 (1976).

[18]P. G. Debenedetti, "Supercooled and glassy water," J. Phys.: Condens. Matter **15**, R1669 (2003).

[19]R. L. Davidchack and B. B. Laird, "Direct calculation of the hard-sphere crystal/melt interfacial free energy," Phys. Rev. Lett. **85**, 4751–4754 (2000).

[20]R. L. Davidchack and B. B. Laird, "Direct calculation of the crystal–melt interfacial free energies for continuous potentials: Application to the Lennard-Jones system," J. Chem. Phys. **118**, 7651–7657 (2003).

[21]J. L. F. Abascal, E. Sanz, R. Garcia, and C. Vega, "A potential model for the study of ices and amorphous water: TIP4P/Ice," J. Chem. Phys. **122**, 234511 (2005).

[22]C. Lobban, J. L. Finney, and W. F. Kuhs, "The structure and ordering of ices III and V," J. Chem. Phys. **112**, 7169–7180 (2000).

[23]J. L. Aragones, L. G. MacDowell, and C. Vega, "Dielectric constant of ices and water: A lesson about water interactions," J. Phys. Chem. A **115**, 5745 (2011).

[24]G. Bussi, D. Donadio, and M. Parrinello, "Canonical sampling through velocity rescaling," J. Chem. Phys. **126**, 014101 (2007).

[25]M. Parrinello and A. Rahman, "Polymorphic transitions in single crystals: A new molecular dynamics method," J. Appl. Phys. **52**, 7182–7190 (1981).

[26]M. Ambler, B. Vorselaars, M. P. Allen, and D. Quigley, "Solid–liquid interfacial free energy of ice Ih, ice Ic, and ice 0 within a mono-atomic model of water via the capillary wave method," J. Chem. Phys. **146**, 074701 (2017).

[27]T. Darden, D. York, and L. Pedersen, "Particle mesh Ewald: An $N \cdot \log(N)$ method for Ewald sums in large systems," J. Chem. Phys. **98**, 10089–10092 (1993).

[28]U. Essmann, L. Perera, M. L. Berkowitz, T. Darden, H. Lee, and L. G. Pedersen, "A smooth particle mesh Ewald method," J. Chem. Phys. **103**, 8577–8593 (1995).

[29]B. Hess, H. Bekker, H. J. C. Berendsen, and J. G. E. M. Fraaije, "LINCS: A linear constraint solver for molecular simulations," J. Comput. Chem. **18**, 1463–1472 (1997).

[30]B. Hess, C. Kutzner, D. van der Spoel, and E. Lindahl, "GROMACS 4: Algorithms for highly efficient, load-balanced, and scalable molecular simulation," J. Chem. Theory Comput. **4**, 435–447 (2008).

[31]A. P. Thompson, H. M. Aktulga, R. Berger, D. S. Bolintineanu, W. M. Brown, P. S. Crozier, P. J. in't Veld, A. Kohlmeyer, S. G. Moore, T. D. Nguyen, R. Shan, M. J. Stevens, J. Tranchida, C. Trott, and S. J. Plimpton, "LAMMPS—A flexible

simulation tool for particle-based materials modeling at the atomic, meso, and continuum scales," Comput. Phys. Commun. **271**, 108171 (2022).
[32]A. R. Tejedor, I. Sanchez-Burgos, E. Sanz, C. Vega, F. J. Blas, R. L. Davidchack, N. D. Pasquale, J. Ramirez, and J. R. Espinosa, "Mold: A LAMMPS package to compute interfacial free energies and nucleation rates," J. Open Source Software **9**, 6083 (2024).
[33]S. Nosé, "A molecular dynamics method for simulations in the canonical ensemble," Mol. Phys. **52**, 255–268 (1984).
[34]W. G. Hoover, "Canonical dynamics: Equilibrium phase-space distributions," Phys. Rev. A **31**, 1695–1697 (1985).
[35]W. Lechner and C. Dellago, "Accurate determination of crystal structures based on averaged local bond order parameters," J. Chem. Phys. **129**, 114707 (2008).
[36]A. B. Weidmann, L. F. Mercier Franco, A. K. Sum, and P. d. A. Pessôa Filho, "Efficient determination of water/ice phase diagram through isenthalpic–isobaric molecular dynamics simulations," J. Phys. Chem. B **129**, 4871–4877 (2025).
[37]S. L. Bore and F. Paesani, "Realistic phase diagram of water from 'first principles' data-driven quantum simulations," Nat. Commun. **14**, 3349 (2023).
[38]M. M. Conde, M. Rovere, and P. Gallo, "High precision determination of the melting points of water TIP4P/2005 and water TIP4P/ice models by the direct coexistence technique," J. Chem. Phys. **147**, 244506 (2017).
[39]D. Frenkel, "Simulations: The dark side," Eur. Phys. J. Plus **128**, 10 (2013).
[40]J. R. Espinosa, E. Sanz, C. Valeriani, and C. Vega, "On fluid-solid direct coexistence simulations: The pseudo-hard sphere model," J. Chem. Phys. **139**, 144502 (2013).
[41]E. G. Noya, C. Vega, and E. de Miguel, "Determination of the melting point of hard-spheres from direct coexistence methods," J. Chem. Phys. **128**, 154507 (2008).
[42]G. Tammann, *Kristallisieren Und Schmelzen* (Barth, Leipzig, 1903), pp. 315–344.
[43]P. W. Bridgman, *Water, In The Liquid and Five Solid Forms, Under Pressure* (Proceedings of the American Academy of Arts and Sciences, 1912), Vol. 47, p. 441.
[44]D. Eisenberg and W. Kauzmann, *The Structures and Properties of Water* (Oxford University Press, London, 1969).
[45]G. Tammann, "Über die grenzen des festen zustandes. IV," Ann. Phys. **337**, 1–31 (1910).
[46]E. Sanz, C. Vega, J. L. F. Abascal, and L. G. MacDowell, "Phase diagram of water from computer simulation," Phys. Rev. Lett. **92**, 255701 (2004).
[47]S. J. Henderson and R. J. Speedy, J. Phys. Chem. **91**, 3069 (1987).
[48]M. A. Gonzalez, C. Valeriani, F. Caupin, and J. L. F. Abascal, "A comprehensive scenario of the thermodynamic anomalies of water using the TIP4P/2005 model," J. Chem. Phys. **145**, 054505 (2016).
[49]M. J. Torrejón, C. Romero-Guzmán, M. M. Piñerio, F. J. Blas, and J. Algaba, J. Chem. Phys. **161**, 064701 (2024).
[50]R. Handel, R. L. Davidchack, J. Anwar, and A. Brukhno, "Direct calculation of solid-liquid interfacial free energy for molecular systems: TIP4P ice-water interface," Phys. Rev. Lett. **100**, 036104 (2008).
[51]R. L. Davidchack, R. Handel, J. Anwar, and A. V. Brukhno, "Ice I_h-water interfacial free energy of simple water models with full electrostatic interactions," J. Chem. Theory Comput. **8**, 2383–2390 (2012).
[52]J. Schmelzer, G. Röpke, and V. B. Priezzhev, *Nucleation Theory and Applications* (Wiley Online Library, 2005), Vol. 76.
[53]X. M. Bai and M. Li, "Calculation of solid-liquid interfacial free energy: A classical nucleation theory based approach," J. Chem. Phys. **124**, 124707 (2006).
[54]B. B. Laird, R. L. Davidchack, Y. Yang, and M. Asta, "Determination of the solid-liquid interfacial free energy along a coexistence line by Gibbs–Cahn integration," J. Chem. Phys. **131**, 114110 (2009).
[55]N. Di Pasquale and R. L. Davidchack, "Suttleworth equation: A molecular simulations perspective," J. Chem. Phys. **153**, 154705 (2020).